Validation of NASA Thermal Ice Protection Computer Codes Part 2 - LEWICE/Thermal

William B. Wright
NYMA, Inc.
Brook Park, OH

Kamel Al-Khalil
Cox & Company, Inc.
New York, NY

Dean Miller
NASA Lewis Research Center
Cleveland, OH

Abstract

The Icing Technology Branch at NASA Lewis has been involved in an effort to validate two thermal ice protection codes developed at the NASA Lewis Research Center: LEWICE/Thermal[1] (electrothermal de-icing and anti-icing), and ANTICE[2] (hot gas and electrothermal anti-icing). The thermal code validation effort was designated a priority during a 1994 "peer review" of the NASA Lewis icing program and was implemented as a cooperative effort with industry.

During April 1996, the first of a series of experimental validation tests was conducted in the NASA Lewis Icing Research Tunnel (IRT). The purpose of this test was to acquire experimental data to validate the electrothermal predictive capabilities of both LEWICE/Thermal and ANTICE. A heavily instrumented test article was designed and fabricated to simulate electrothermal de-icing and anti-icing modes of operation. Thermal measurements were then obtained over a range of test conditions for comparison with analytical predictions.

This paper will present the comparison between the experimental data and the most recent version of the LEWICE/Thermal computer code, LEWICE 1.6/Thermal (alpha version). The paper will also provide a description of the model used in this code and the improvements which have been made to this code since its creation in 1991. Several capabilities have been added to this code especially within the last year in order to better model the phenomena observed in the April 1996 test.

Nomenclature

α angle of attack, degrees
k   thermal conductivity, W/m/$^\circ$K
LWC   liquid water content, g/m^3
MVD   median volume drop diameter, μm
Q   heater wattage, W/in^2
V   velocity, mph
T   temperature, $^\circ$F
x   surface direction, m
y   direction normal to surface, m
t   time, seconds

Introduction

In 1994 the Icing Technology Branch at the NASA Lewis Research Center conducted a "peer review" process to prioritize its programs based on technological needs identified by industry partners. The need for validated thermal ice protection computer codes was identified as a priority during this peer review process. As a result, NASA Lewis established an experimental program to validate two thermal ice protection codes developed by NASA Lewis: LEWICE/Thermal (electrothermal de-icing and anti-icing) and ANTICE (hot gas and electrothermal anti-icing).

Two experimental tests were designed for the initial validation activity. The first test utilized an airfoil

with an electrothermal ice protection system and will be used to validate the electrothermal de-icing and anti-icing capability of LEWICE/Thermal and the electrothermal anti-icing capability of ANTICE. This test was conducted in April 1996 and is the subject of this paper. The second experimental test in the thermal code validation effort will utilize an airfoil with a hot gas ice protection system and will be used to validate the hot gas anti-icing predictive capability of ANTICE. This second test is currently planned for a 2-3 week time period in 1997.

This paper will present a description of the LEWICE/Thermal model with an emphasis on recent developments and provide several comparisons with the data taken in the IRT. This paper is the second of three papers on this test. The first paper[3] will present an overview of the test and a description of the test techniques and data taken. The third paper in the series[4] will provide description of the ANTICE model and comparison with the anti-icing results.

Background

The removal and/or prevention of ice on aircraft components is vital to aircraft performance and operation. Even small amounts of ice can have disastrous consequences. Because of this, several methods of ice prevention and removal have been designed. Methods of ice control can be arranged into two broad categories: anti-icing methods and de-icing methods. Anti-icing methods are concerned with the prevention or minimization of ice buildup on protected surfaces. De-icing methods are concerned with ice removal after and during ice build up.

A widely used method for either anti-icing or de-icing aircraft components is with an electrothermal pad. By this method, heater mats are installed beneath the skin of a wing surface surrounding the leading edge as shown in Figure 1. Thermal energy in the form of conducted heat destroys the adhesion force at the ice-surface interface. Aerodynamic forces then sweep the ice from the surface. When more heat is supplied, the ice will melt completely and runback to unheated regions. If enough heat is supplied, the water will not freeze on the surface, creating an anti-icing condition.

Over the years, several researchers have developed computer codes which model thermal deicers[5-9]. These early codes modeled only the de-

icing process after ice had formed but did not model the ice accretion process itself. Wright[10] was the first to model the complete deicing process with ice accretion in an effort funded by NASA Lewis. This code was the first version of LEWICE/Thermal[11]. This code combined the deicer code developed by Wright[9] with the capabilities of the LEWICE code[12].

LEWICE solves for the two-dimensional potential flow around a body. It then calculates water droplet impingement limits, water collection efficiency and the external heat transfer coefficient. This information is input into a mass and energy balance to find the ice growth on an unheated airfoil. The most recent release of this code, LEWICE 1.6[13-16], incorporates greater flexibility with respect to adding other capabilities through its modular design.

One such capability would be the incorporation of a code to model thermal deicers. This process was carried out in the first version of LEWICE/Thermal[11], but transferring updates to LEWICE into this code proved difficult. The current version of this code, called LEWICE 1.6/Thermal (alpha version), allows for future upgrades to be incorporated in a more streamlined manner. It also allows the thermal deicer to be used in other NASA icing codes without modification. For example, a grid-based Naviér-Stokes flow solver can now be used in conjunction with the thermal code by taking a LEWICE 1.6/NS[17] code and combining it with the LEWICE 1.6/Thermal code using a unix 'make' file or using a standard PC fortran compiler. In previous versions of LEWICE, substantial changes would have to be made to the code to integrate additional modules such as the thermal deicer module or a Naviér-Stokes code.

LEWICE 1.6[13-16] is composed of the following seven modules as shown in Figure 2: 1) main.f - main program which calls other routines; 2) flow.f - in the baseline model, this is the S24Y Hess-Smith potential flow code; 3) vedge.f - calculates compressible edge velocities and stagnation point; 4) traj.f - calculates particle trajectories and collection efficiency; 5) bdy.f - performs integral boundary layer and calculates external convective heat transfer coefficient; 6) ice.f - performs energy and mass balance on surface and computes ice growth rate at each control volume; 7) geom.f - creates a new (iced) geometry based on the ice growth rate and time step. For a

variable time step, the time step is based on the maximum ice growth rate and the limiting thickness.

Thermal Deicer Module

The LEWICE/Thermal code calculates the 2D transient (time-dependant) heat transfer in a composite body. It can handle multiple layer bodies, composite materials with anisotropic ($k_x \neq k_y$) material properties, individually controlled heaters with separate on/off times and power densities, as well as ice growth with or without heaters, ice shedding, water runback. It can also function as an ice accretion code similar to LEWICE. The original deicer code was created using LEWICE 1.0 and has been documented in several reports[1,10,11].

LEWICE 1.6/Thermal is designed to combine the best features of both codes and improve modularity for future upgrades. In this case, ice.f ice accretion module is replaced by iced.f which is an ice accretion/deicer module. The same set of variables such as collection efficiency and heat transfer coefficient are transferred into both ice.f and iced.f. Similarly, the variables transferred out of each module (ice or iced) are also the same. Therefore, the iced.f module will produce the same results as ice.f if all thermal heaters are turned off. Using this module, a multi-element thermal deicing code or a Naviér-Stokes deicing code can be created in minutes by running the appropriate unix 'make' file or through compiling the modules on a PC. However, any future upgrades to the ice.f module, such as an improved runback routine or additional energy balance terms, will have to be programmed into both the ice.f module and the iced.f module.

The following features have been added to the thermal deicer code since its creation (LEWICE/Thermal 1.0[11]):

1) The thermal module is fully integrated with the other code modules and can be run in 'heater off' mode. In this mode, it will respond exactly like LEWICE 1.6 and produce very similar ice shapes, even for multiple time-steps.

As mentioned earlier, this update allows the thermal deicer module to be used with any flow code which has been interfaced with version 1.6.

2) It can perform multiple-time step ice accretions before heaters turn on, while they are on or after they are turned off and can recalculate flow after shedding incidents. Previously, only single time step flow solutions were used with version 1.0.

3) It incorporates improvements made to energy balance and advanced runback features found in version 1.6 but not in version 1.3 or version 1.0.

4) It supports full ice shedding, or partial (node-by-node) ice shedding. This model uses a macroscopic force balance either on the total shape or on the ice at each control volume. If the adhesion force (determined by experimental correlation as a function of temperature) is less than the aero forces, then the ice (or the ice at that control volume) will shed. Because of this, surface water will shed in the code as it has no adhesion force. As a result, all the cases run to date will not have any residual ice growth past the heaters until this feature is added. This feature will be available when the code is officially released.

5) Stability of the code has been greatly improved, allowing analysis of more cases and more complex cases. This result is mostly due to the integration of version 1.6 instead of version 1.0. The thermal 1.6 version has not crashed for any case run to date.

6) It can track shed ice particle trajectories by accessing portions of the particle trajectory code. (Assumes shed ice particles are spherical.) This feature is very simplistic and does not check to see if the ice particle travels through the airfoil.

7) It can run heaters on before accretion begins (pre-heating) or after exiting from cloud (after spray off). Previously, the icing environment could not be turned off during a run.

8) Each heater can be individually controlled by on/off cycle or individually controlled to a specified temperature range. You can mix modes and have parting strip temperature controlled and the others have a specified on/off cycle. This feature reflects how some deicers are controlled in reality.

9) Heaters can have a thermal resistance which depends on temperature. Some innovative deicer designs use heater materials where the thermal resistance is a function of temperature. It would be a trivial modification to extend temperature dependance of the thermal resistance to other layers. Feedback from industry would be useful on the value of this feature.

10) Heater design can be completely different from one body to another in a multi-body/multi-element simulation. For example, this allows the user to model ice protection on a slat while the other ele-

ments are left unprotected. However, this feature requires that the user create a separate input file for each body.

11) Parting strip heater can be specified to have an offset from the leading edge (previously 'fixed' on the leading edge). This feature was added to model the actual case where the center of the parting strip heater on the test article was offset 0.18" from the leading edge due to manufacturing difficulties.

12) For more seamless integration with other LEWICE codes and for future versions, all units in LEWICE 1.6/Thermal are metric ($T=^{\circ}K$, $Q=kW/m^2$, etc.). Therefore the users of version 1.0 will need to modify their input data files to be compatible with version 1.6.

13) Output to a post-processor plot package (PLOT3D[18]) has been integrated with the code and selectable from input file. This allows the user to create contour plots which show much more detail than the 'thermocouple style' temperature vs. time plots can show. Examples of these plots are shown later in this paper.

14) The one dimensional steady-state 'fast solution' from LEWICE 1.6 has been incorporated in the model. Input data comes from the main deice file. This 'fast solution' is used to get an idea of the power requirements to reach steady state. An analysis is planned which will compare this simplistic solution with the more rigorous LEWICE/Thermal solution so the user knows the accuracy of this approximation. That analysis has not been done yet and will not be presented in this paper.

15) Thermal version 1.6 outputs more than one data style at a time. Previously, if temperature vs. time output (at a specified x,y location) was identified, the code could not print out temperature vs. x (at a specified y and t) or temperature vs. y (at a specified x and t) in the same run. This is useful for printing out surface temperature as a function of x at time1, time 2, etc. while printing out thermocouple temperature predictions in the same run. The PLOT3D compatible files are also output in the same run. Examples of all output types will be presented in this paper. It should be noted that here x refers to the wrap distance around the airfoil and y refers to the distance normal to the surface, not the global x,y coordinates.

Results

The test article was a NACA0012 airfoil with a 72 inch span and a 36 inch chord. The composite leading edge had seven independently controllable heater zones as shown in Figure 3. The material properties of the heater mat are given in Table 1. Heater zone A (parting strip) was on continuously for all the runs. The other heaters were cycled using various power settings and on/off times.

Development of the test matrix involved the selection of two different types of parameters: icing parameters (To, LWC, MVD, etc.) and electrothermal ice protection system parameters (heater power level and heater zone on/off time). The combination of both sets of parameters resulted in an extremely large number of possible test parameter combinations. Consequently, the test was restricted to a few different icing conditions and a wider variety of ice protection parameters.

Several icing conditions were selected for this test, however two in particular were designated as 'anchor point' conditions:

$T_o=20 ^{\circ}F$, V=100 mph, LWC=0.78 g/m^3, MVD=20 μm

$T_o=0 ^{\circ}F$, V=100 mph, LWC=0.78 g/m^3, MVD=20 μm

At each of these two conditions, ice protection system parameters were varied. Additional icing conditions were produced by varying only one of the parameters above. This paper will present comparisons for the 'anchor point' conditions only.

The primary parameters for the ice protection system were the heat flux applied to each heater zone and the time sequencing (on/off times) of each heater. The first set of runs in the tunnel test were used to estimate the wattages and on/off times appropriate for each of the 'anchor point' conditions. A heater cycle of 10 sec. on and 110 sec off was found to be the most optimal during this initial phase and was used as the baseline case for subsequent runs during this test.

The baseline or 'anchor point' of the heater deicing cycle (10 sec. on and 110 sec off) was used as the selection criteria for comparison with the code results. This resulted in the selection of nine cases for the initial validation attempt. Of these nine cases, four were selected for presentation in this paper as representative of the results. The other cases were ran for validation purposes and will be available when the experimental data is released this coming year

on a CD-ROM. The four cases selected are listed in Table 2.

The first case had the following conditions:

Htr. A = 5 W/in^2, B,C = 10 W/in^2, D-G = 8 W/in^2

T_o=20 °F, V=100 mph, LWC=0.78 g/m^3, MVD=20 μm

Case 1 will be used to illustrate the various methods which can be used to look at the results. The other cases will only show comparisons to the test data.

There are four types of temperature output available in LEWICE/Thermal to aid the user in interpreting the results. The most commonly used option is to output temperature vs. time at a given x,y location. These temperatures are used to compare the results to experimental data. For all cases, only temperatures for heaters A (Parting strip), B and D will be shown. Heater C is identical to heater B since the data is nearly symmetric. Similarly, heater E is directly opposite to heater D and the results are very similar. Heaters F and G show very similar results to heaters D and E and also are not shown. During the test, it was noticed that the parting strip heater was not centered on the leading edge as designed, but was shifted to one side by 0.18". However, this shift did not alter the symmetry of either the experimental or numerical results. Therefore, only one side is presented.

Figure 4 shows the first type of output for Case 1. This figure compares the heater temperatures predicted with those measured by RTDs underneath the heaters. Since the RTD was directly beneath the heater, the LEWICE/Thermal temperature at the heater/epoxy interface was used for comparison. This result compares reasonably well to the data. The parting strip heater shows a different response when heaters B and C turn on and the code does not show the correct cooling cycle for heaters B and D after they turn off. Both phenomena are attributed to the method by which LEWICE/Thermal models shedding and runback water.

When the initial ice shape sheds (indicated by the rise in temperature over heater A), the code will continuously shed the runback water rather than allowing it to flow over the other heaters and refreeze. The flow of surface water has a cooling effect which explains why the experimental data shows heater A cooling to its previous level after heaters B and C turn off. This is seen more clearly in Figure 5 which shows the first cycle of data only and Figure 6 which shows the second data cycle. Figure 6 also shows an underprediction of heater B in subsequent cycles. Once the code has been corrected to model the runback separate from shedding, the cases will be run again to determine if this is the true cause of the temperature difference.

Figure 7 shows the temperature comparison for Case 1 at the abrasion shield. A type-T thermocouple was placed on the underneath surface of the abrasion shield over each heater. For clarity, only the first cycle is shown on this and subsequent plots. This figure shows good comparison with the data except for heater B. The difference in this result is attributed to an error in the runback and shedding model. LEWICE/Thermal uses the shedding routine to remove any ice or water which does not adhere to the surface. Surface tension effects are not included. Therefore, runback water will be shed rather than flow to the next control volume where it might freeze. This problem is unique to the thermal code, since LEWICE does not have an ice shedding model. This correction will be included when the code is officially released. The result of this error causes this temperature to be underpredicted.

Figure 8 shows the code comparison with thermocouples located on the inside surface of the airfoil at the base of the foam layer. These temperatures represent the foam temperatures underneath heaters A, B and D. The comparisons here are very good because the effect of the surface water model is dampened.

As stated earlier, this is the only type of output from the code which can be easily compared to the experimental results. For design purposes, it may be useful to plot the data in different formats. Figure 9 shows an example of a potentially useful format. In this figure, the temperature is plotted as a function of distance from the leading edge at the ice/metal surface for several times. This plot can show cold spots where additional heating may be required to melt the ice. It also shows the time needed to get the entire surface over a particular heater to go above freezing.

The first curve, at 100 seconds, in this figure is the steady-state temperature distribution immediately before the heaters B and C turn on. For reference, the 32°F line is shown as well as the heater widths in the boxes at the bottom of the plot. The second curve, at 105 seconds, shows the distribution at the midpoint of the on-time for these heaters while the third curve, at 110 seconds, shows the distribution

immediately before these heaters turn off. This curve shows the axial conduction of heat from heaters B and C to heater A and to a lesser extent to heaters D and E.

Figure 10 shows the same style plot during the second half of the deicer cycle. Temperature is again plotted as a function of wrap at the ice/metal interface. In this case, heaters B and C are off and heaters D through G are on. The times plotted show the results when B and C turn off, at the midpoint of the on cycle for heaters D-G, and at the end of the on-cycle for heaters D-G. These two figures show fairly uniform temperature over the heaters. This is important from a comparison standpoint. It is nearly impossible to determine the axial location of the thermocouples and RTD measurement devices. The test planned to have the measurement location at the center of the heater, but manufacturing difficulties make it difficult to know if this was achieved. These two plots show that the measurement location does not have to be at the exact center of the heater to correctly represent the heater temperature.

Another measurement style is shown in Figure 11. In this case, the temperature profile normal to the surface is plotted for heater B at the same times as shown in Figure 9. This temperature profile is a plot showing the temperature distribution from the bottom of the deicer pad (y=0) through the heater, abrasion shield and any ice that may exist at that chordwise location. This type of plot can be used to show that a majority of the heat is transferred to the upper surface and to ensure that there are no 'hot points' which could cause the deicer to overheat.

The final type of plot style is shown in Figure 12. This figure shows the temperature contours [T(x,y)] in the airfoil at a particular time. This plot is created by reading the output from LEWICE/Thermal into PLOT3D, a standard unix plotting package. The output could easily be changed to work with any plotting package however. Some file manipulation is required to transform the code output to PLOT3D form. This procedure will be described in the user manual to be published later this year.

This plot shows the hot and cold spots in the deicer which can be useful for design purposes. This figure shows the contour plot 130 seconds into the run. At this point, heaters D through G have been on for 10 seconds and are about to turn off. On the original color plot, residual heat from heaters B and C's on-cycle can still be seen. This plot also shows the

extent of chordwise conduction better than other plot styles. It also shows the effect of the heater offset very well. During the test, the parting strip heater was found to be offset from the leading edge by 0.18". This was modeled in code for all of the comparisons. This offset did not have a large effect on either the experimental temperature measurements or in the code since the temperature over each heater was essentially uniform. Results were nearly symmetric, therefore all of the comparisons only show one side of the data.

The conditions for Case 2 were:

Htr. A = 5 W/in^2, B,C = 7 W/in^2, D-G = 7 W/in^2

T_o=20 °F, V=100 mph, LWC=0.78 g/m^3, MVD=20 μm

Case 2 has the same tunnel conditions as Case 1 but with lower wattages on heaters B through G. Throughout the test, several heater wattages and cycles were used to provide a diverse set of conditions for this validation effort. In this case, the lower wattages create a case where the ice does not shed until the end of the cycle. Figure 13 shows the comparison of heater temperatures for heaters A, B and D. The comparison is very similar to Case 1. The parting strip temperature is overpredicted slightly which also causes more residual heating downstream. The peak temperatures of the deicer cycles are predicted better than the first case.

The comparison of surface temperatures and substrate (foam) temperatures for these three locations is shown in Figures 14 and 15. The comparisons here are also slightly better than Case 1. Since the wattages are not as high in Case 2, the temperature does not rise as much which causes the difference in prediction to be less as well.

The conditions for Cases 3 and 4 were:

Case 3

Htr. A = 10 W/in^2, B,C = 12 W/in^2, D-G = 10 W/in^2

T_o=0 °F, V=100 mph, LWC=0.78 g/m^3, MVD=20 μm

Case 4

Htr. A = 12 W/in^2, B,C = 16 W/in^2, D-G = 15 W/in^2

T_o=0 °F, V=100 mph, LWC=0.78 g/m^3, MVD=20 μm

Cases 3 and 4 have the same tunnel conditions as the first two cases, except that the tunnel temperature is 0°F instead of 20°F. Because of the lower temperature, higher wattages were used for these cases. During the test, the heaters wattages were varied to show the deicer performance for various settings.

Figure 16 shows the comparison of heater temperatures for Case 3. The comparison for heaters B and D are very good, but the code significantly underpredicts the temperature for heater A, the parting strip. Additionally, the code shows a faster rise to steady state than the experiment.

The reason for this discrepancy in prediction is seen in Figure 17 which shows the comparison of the surface temperatures for this case. In the experiment, the ice was successfully shed from heater A and the temperature rose above 32 °F. In the code prediction, the ice did not melt and the surface temperature remained at 32 °F as it predicted that there was not enough heat to melt the ice. Since the ice remains at the lower temperature, it keeps the heater at a lower temperature as well since most of the heat is going into melting the ice.

There could be many factors which could cause this difference. Discrepancies between the actual and predicted heat transfer coefficients and improper modelling of the shedding/runback criteria are some of the potential problems. It should be noted that heater D, which is beyond the impingement limit, shows very good agreement. This highlights that there is a problem in the physical model and the discrepancy is not an error in thermal properties or a measurement error.

Figure 18 shows the comparison of substrate (foam) temperatures for this case. The difference is somewhat masked here since this location is farthest from the ice surface. It also shows that, especially for the heater B location, more heat is being transferred to the inner surface of the airfoil as the melting process partially blocks heat transfer to the surface.

Case 4 has the same tunnel conditions as Case 3 but with higher heater wattages. The comparisons are shown in Figures 19-21. Again, there is significant underprediction by the code especially for the parting strip heater locations. As shown in Figure 20, this is again a result of the code taking too long to melt the ice. In this case, the higher wattages are just enough to cause a shedding event, which is shown by the sudden increase in temperature at 111 sec. when heater B is at maximum power and heater D is just turning on. After this time, the parting strip heater prediction is closer to the experimental values. It does not fully recover to the experimental values because the ice did not melt elsewhere, as evidenced by the surface temperature prediction for heater B. The substrate temperature comparison is shown in Figure 21 and shows similar trend as shown in Case 3.

Conclusions

A test was ran in the NASA Lewis Icing Research Tunnel for the purpose of validating the thermal ice protection codes developed by and for the NASA Lewis Icing Branch. Comparisons to thermocouple results for this test were made with a new version of the LEWICE/Thermal Deicing code. This code combines the features of the LEWICE 1.6 ice accretion code with a model of a thermal deicer which formed the basis of the original LEWICE/Thermal Code. This new version of the deicer code has many new features described in the paper. In addition, it is more versatile in that the LEWICE/Thermal 1.6 module can be easily ported to other versions of LEWICE and used without extensive user development.

Results from the comparison showed that the code performed well for the warmer 20°F cases but showed significant underprediction of the parting strip temperature for the colder 0°F cases. Work continues on this code to improve the criteria for water runback and ice/water shedding. An official release of this code to users along with a new users manual is expected by mid-1997.

References

1) Wright, W. B. Keith, T.G. and DeWitt, K.J., "Numerical Analysis of a Thermal Deicer," AIAA-92-0627), Jan. 1992.

2) Al-Khalil, K.M., "Numerical Simulation of an Aircraft Anti-Icing System Incorporating a Rivulet Model for the Runback Water," PhD Dissertation, University of Toledo, Toledo, Ohio, Jan. 1991.

3) Miller, D. et. al.,"Validation of NASA Thermal Ice Protection Computer Codes: Part 1 - Program Overview," NASA TM 107397, AIAA-97-0049, Jan. 1997.

4) Al-Khalil, K.M., Miller, D. and Wright, W.B., "Validation of NASA Thermal Ice Protection Computer Codes: Part 3 - Thermal Anti-Icing," AIAA-97-0051, Jan. 1997.

5) Gent, R.W. and J.T. Cansdale, "One-Dimensional Treatment of Thermal Transients in Electrically Deiced Helicopter Rotor Blades," RAE TR 80159. 1980.

6) Masiulaniec, K.C., "A Numerical Simulation of the Full Two-Dimensional Electrothermal Deicer

Pad," PhD Dissertation, University of Toledo, Toledo, Ohio, June 1987.

7) Wright, W.B., Keith, T.G. and De Witt, K. J., "Transient Two-Dimensional Heat Transfer Through a Composite Body with Application to Deicing of Aircraft Components," AIAA-88-0358, Jan. 1988.

8) Henry, R., "Etude du Fonctionment d'un Degivreur Electrique: Modelisation et Mesure en Soufflerie Givrante de Temperature Parietale par Thermographie Infrarouge," PhD Dissertation, Blaise Pascal University, Clermont-Ferrand II, France, Sept. 1989.

9) Wright, W. B., "A Comparison of Numerical Methods for the Prediction of Two-Dimensional Heat Transfer in an Electrothermal Deicer Pad," MSc Thesis, University of Toledo, Toledo, Ohio, Feb. 1988.

10) Wright, W. B., "Simulation of Two-Dimensional Icing, De-Icing and Anti-Icing Phenomena," PhD Dissertation, University of Toledo, Toledo, Ohio, Dec. 1991.

11) Masiulaniec, K.C. and Wright, W.B., "User's Manual for the NASA Lewis Ice Accretion/Heat Transfer Prediction Code with Electrothermal Deicer Input," NASA CR 4530, July 1994.

12) Ruff, G.A. and Berkowitz, B.M., "Users Manual for the NASA Lewis Ice Accretion Prediction Code (LEWICE)," NASA CR 195387, May 1990.

13) Wright, W.B., "Users Manual for the Improved NASA Lewis Ice Accretion Code LEWICE 1.6," NASA CR198355,June 1995.

14) Wright, W. B. and Bidwell, C. S., "Additional Improvements to the NASA Lewis Ice Accretion Code LEWICE," NASA TM (AIAA-95-0752), Jan. 1995.

15) Wright, W.B., Bidwell, C. S., Potapczuk, M. G. and Britton, R. K., "Proceedings of the LEWICE Workshop," June 1995.

16) Wright, W.B., "Capabilities of LEWICE 1.6 and Comparison with Experimental Data," presented at the SAE/AHS International Icing Symposium, Sept. 1995.

17) Potapczuk, M.G., Al-Khalil, K.M., Velazquez, M.T., "Ice Accretion and Performance Degradation Calculations with LEWICE/NS," NASA TM-105972, AIAA-93-0173, Jan. 1993.

18) Walatka, P. P., et. al., "PLOT3D User's Manual," NASA TM 101067, March 1990.
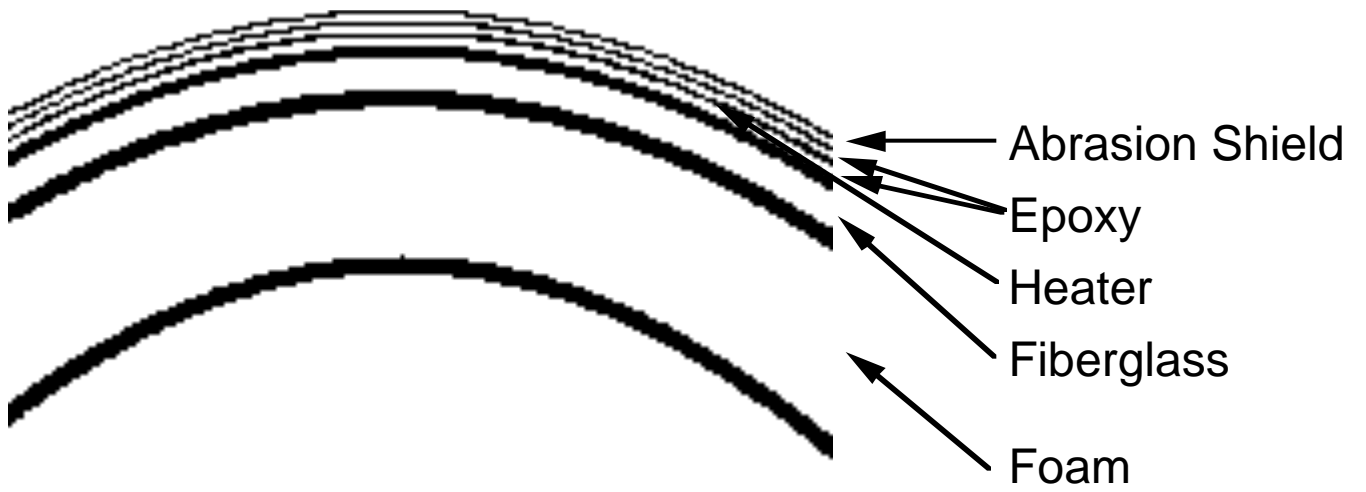
FIGURE 1. Airfoil Equipped with an Electrothermal Deicer
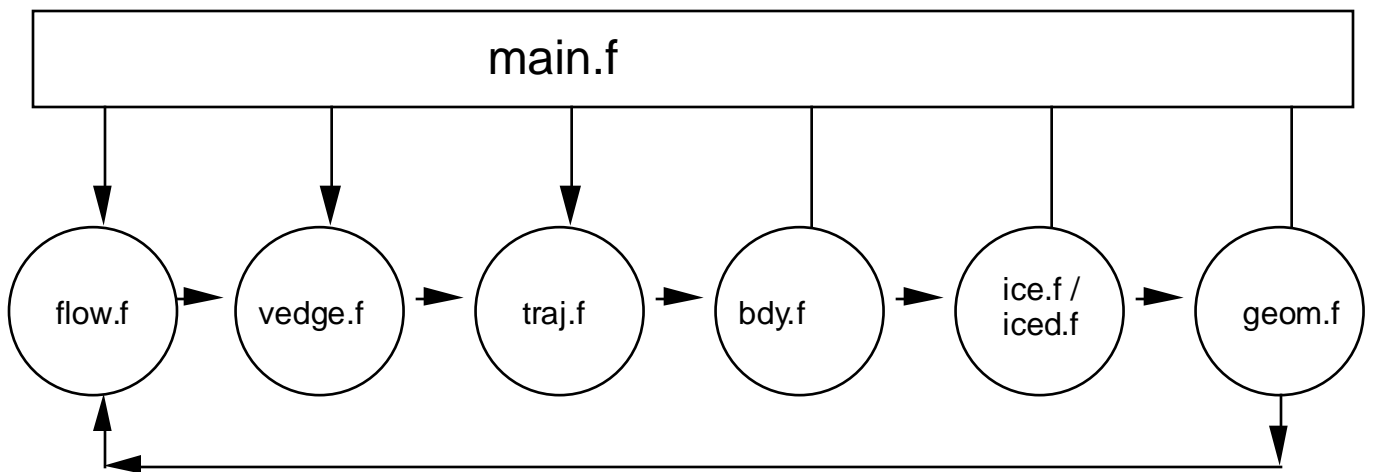
FIGURE 2. Diagram of LEWICE 1.6 with Thermal Code Extension shown

TABLE 2.   Conditions Used for Initial Validation

Case 1	Case 2	Case 3	Case 4
Htr. A = 5 W/in^2	5 W/in^2	10 W/in^2	12 W/in^2
B,C = 10 W/in^2	7 W/in^2	12 W/in^2	16 W/in^2
D-G = 8 W/in^2	7 W/in^2	10 W/in^2	15 W/in^2
T$_o$=20 °F	20 °F	0 °F	0 °F
V=100 mph	100 mph	100 mph	100 mph
LWC=0.78g/m^3	0.78g/m^3	0.78 g/m^3	0.78 g/m^3
MVD=20 μm	20 μm	20 μm	20 μm

FIGURE 3. Schematic of Heater Zones

TABLE 1.   Material Properties of Thermal Deicer

Layer	Material	Thickness mm	Conductivity W/m/K	Diffusivity m^2/s*10^7
1	Foam	3.43	0.121	1.65
2	Fiberglass	0.89	0.294	1.04
3	Elastomer	0.28	0.256	1.50
4	Heater	0.013	41.0	120.0
5	Elastomer	0.28	0.256	1.50
6	Ab. shield	0.20	16.3	40.6
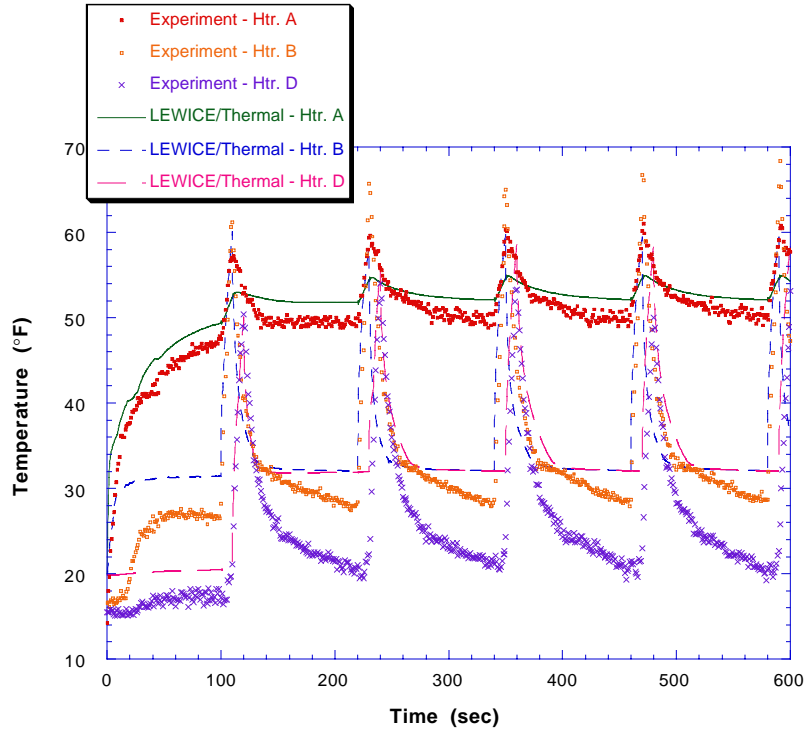
FIGURE 4. Comparison of Heater Temperatures for Case 1
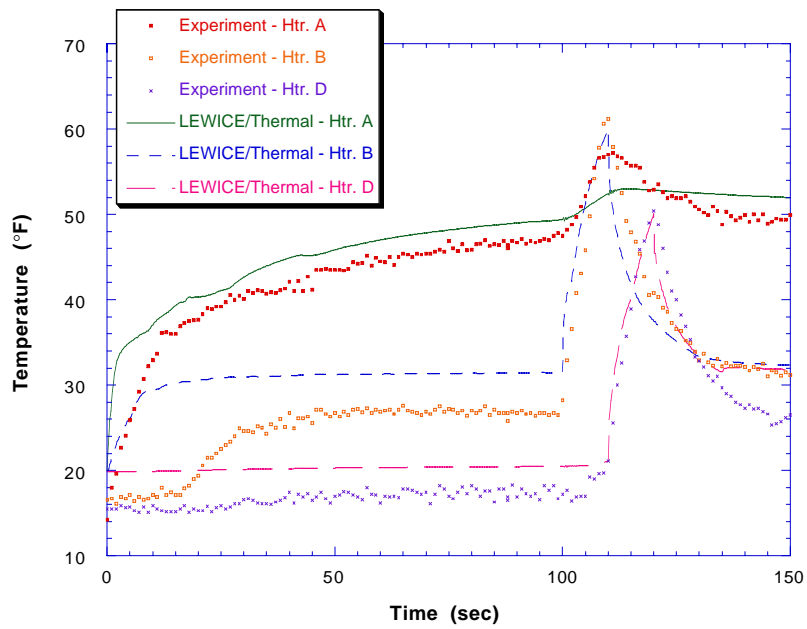
FIGURE 5. First Heater Cycle for Case 1

11
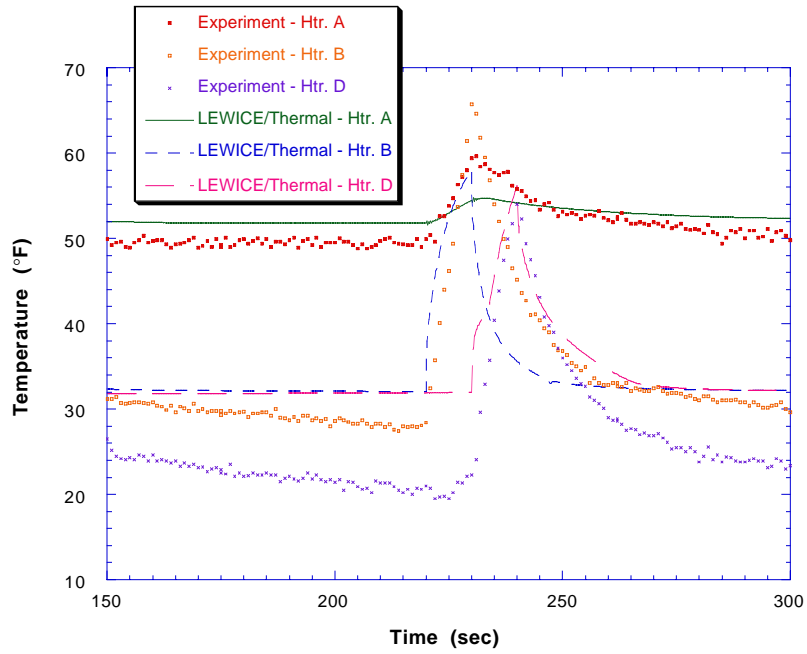
FIGURE 6. Second Heater Cycle for Case 1
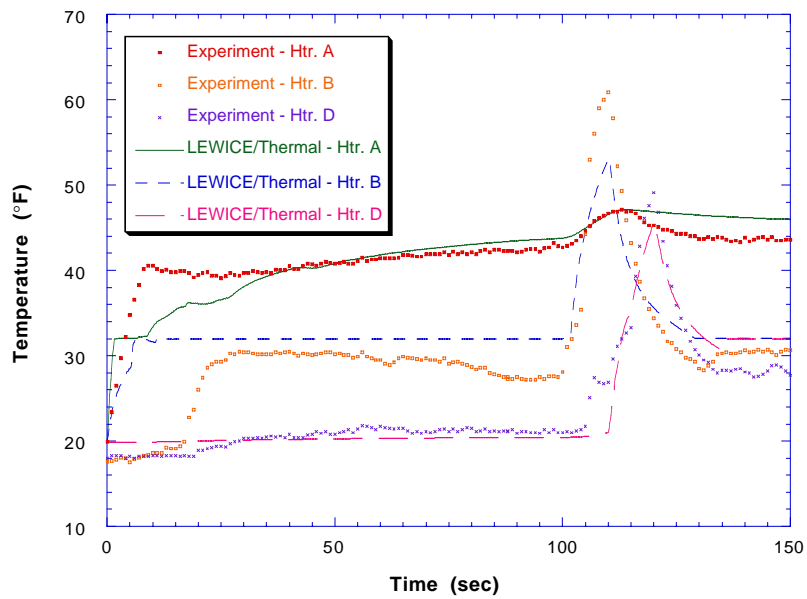
FIGURE 7. Comparison of Surface Temperature for Case 1
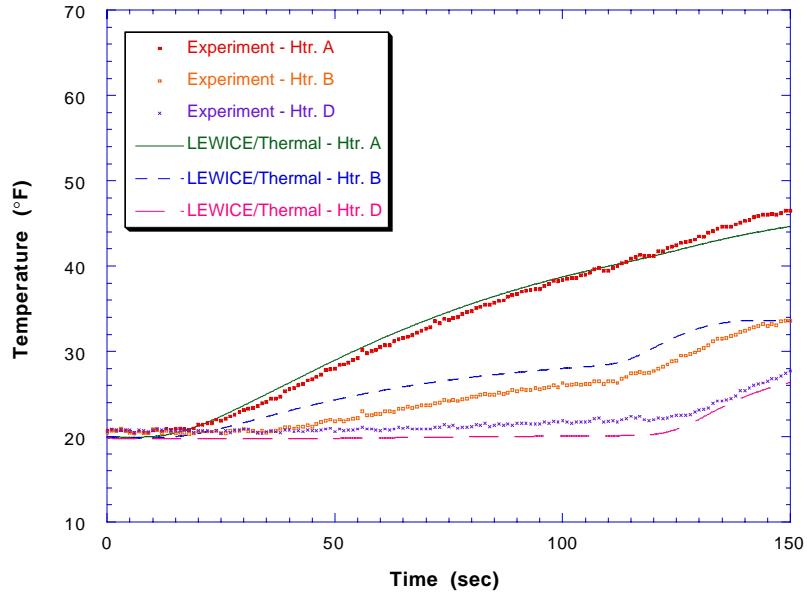
FIGURE 8. Comparison of Foam Temperature for Case 1
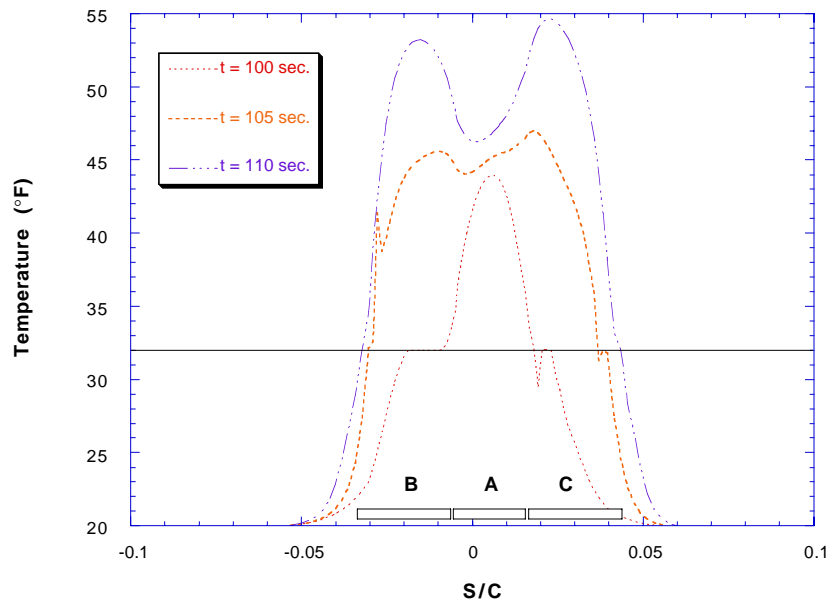
FIGURE 9. Temperature vs. Surface Distance with Heaters A, B, C on

13
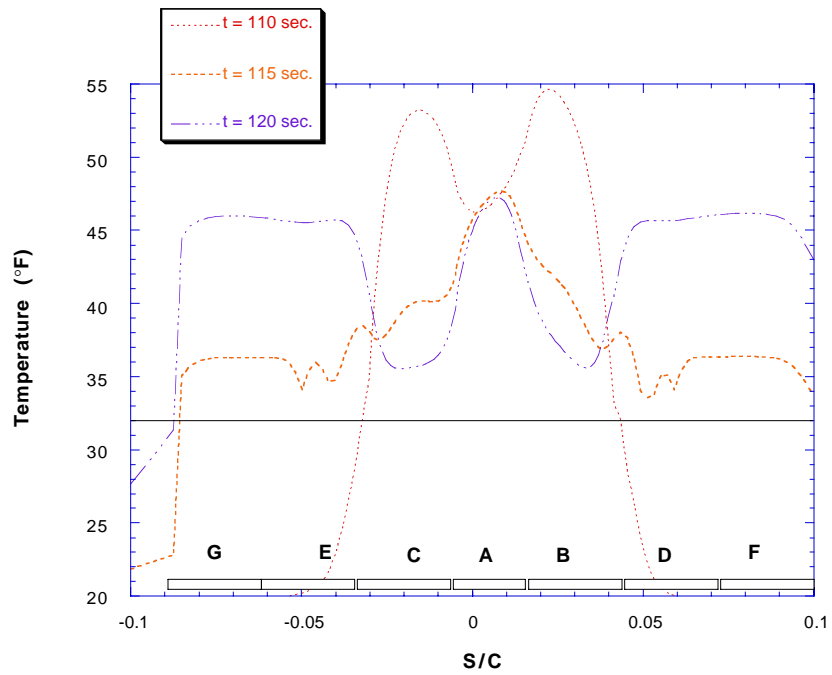
FIGURE 10. Temperature vs. Surface Distance with Htrs A, D- G on.
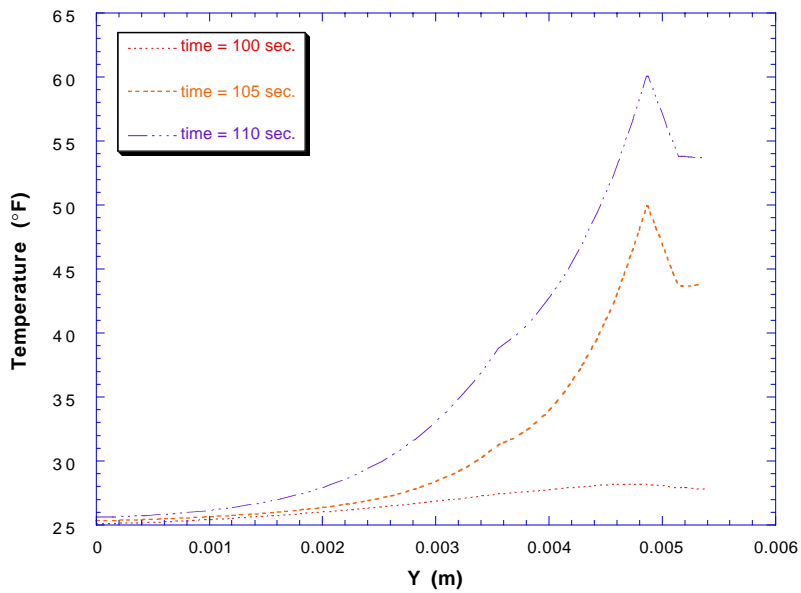
FIGURE 11. Temperature Distribution Normal to the Surface for Heater B

14

FIGURE 12. Thermal contour plot after 120 sec. for Case 1
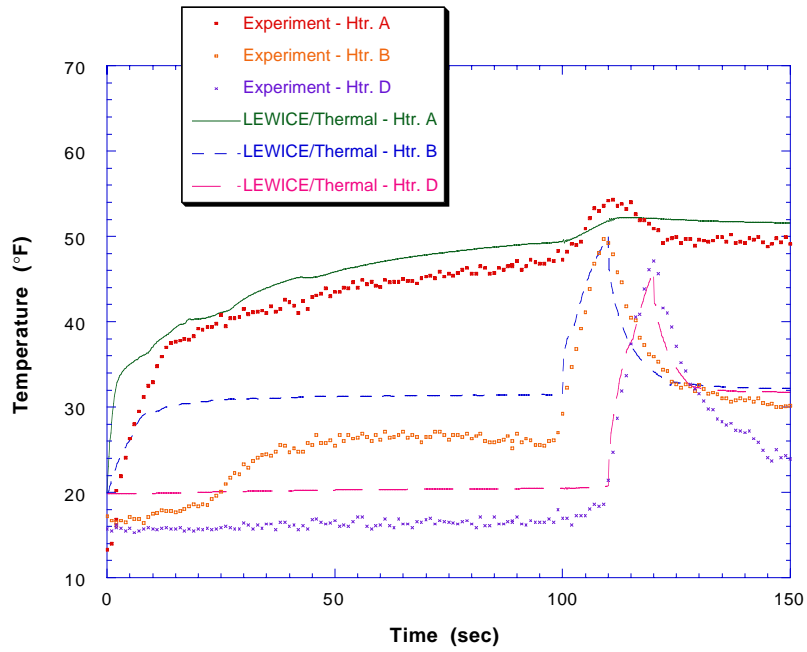
FIGURE 13. Heater Temperature Comparison for Case 2
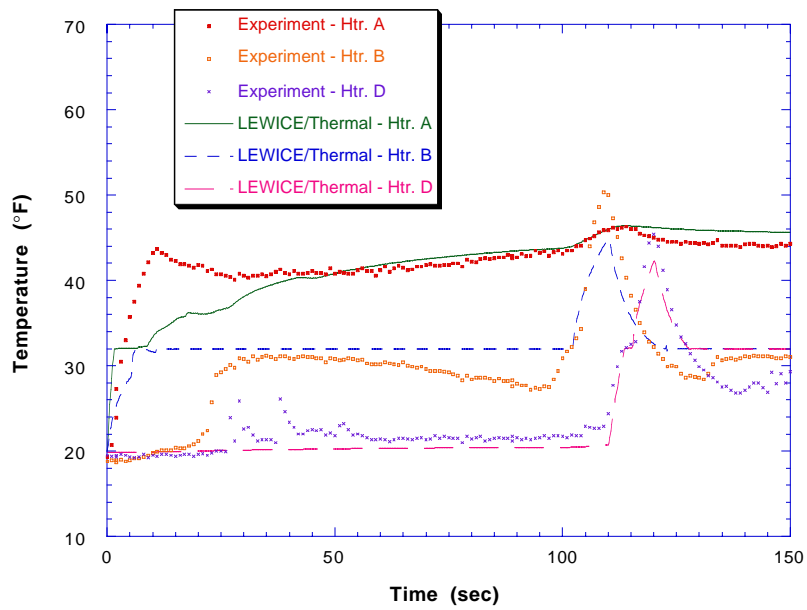
FIGURE 14. Surface Temperature Comparison for Case 2
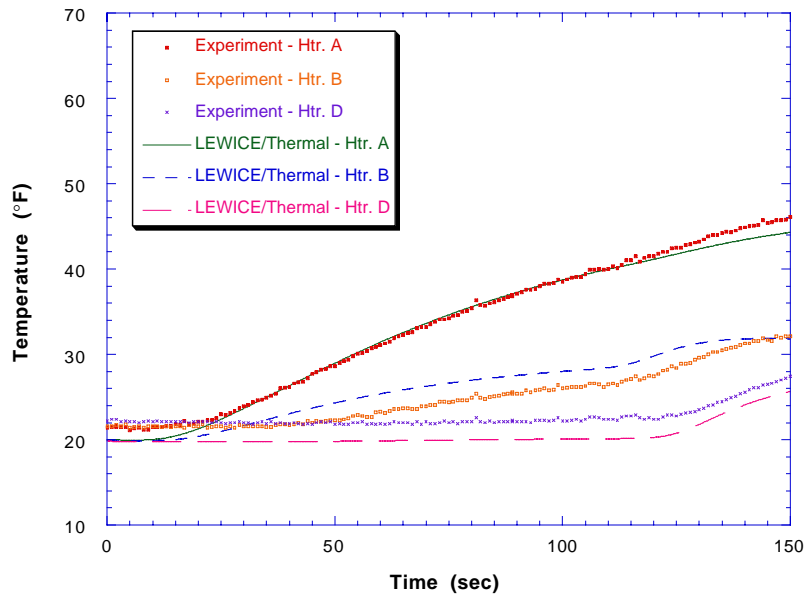
FIGURE 15. Foam Temperature Comparison for Case 2
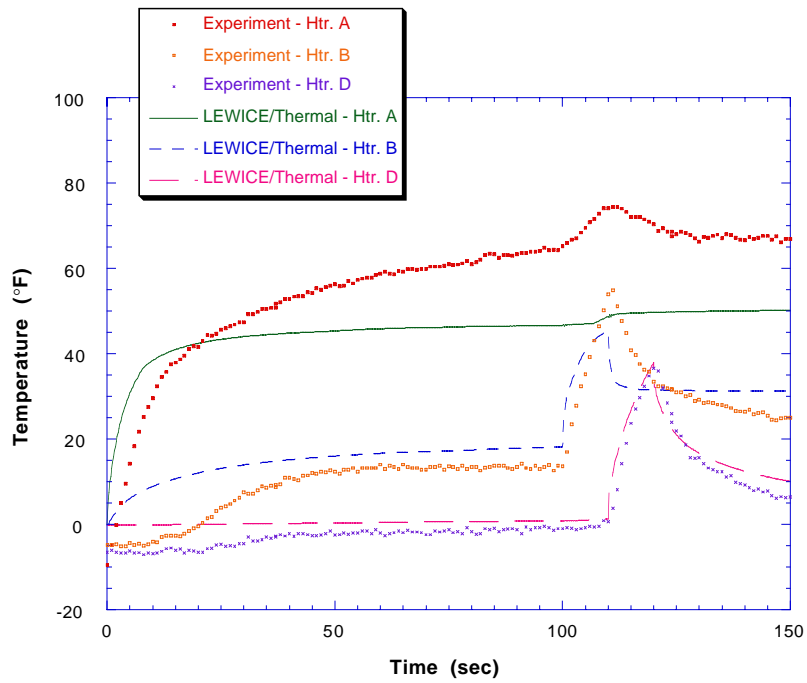
FIGURE 16. Heater Temperature Comparison for Case 3
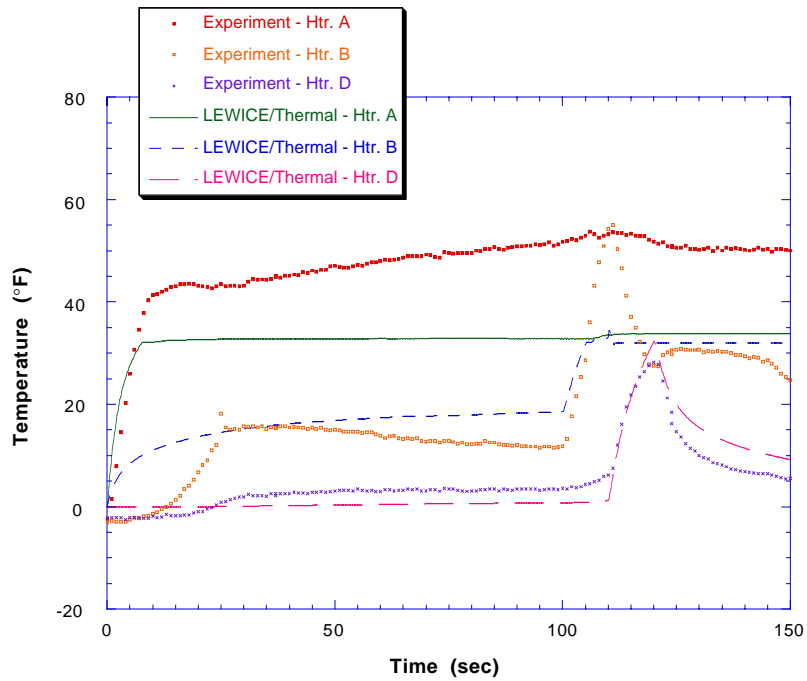
FIGURE 17. Surface Temperature Comparison for Case 3
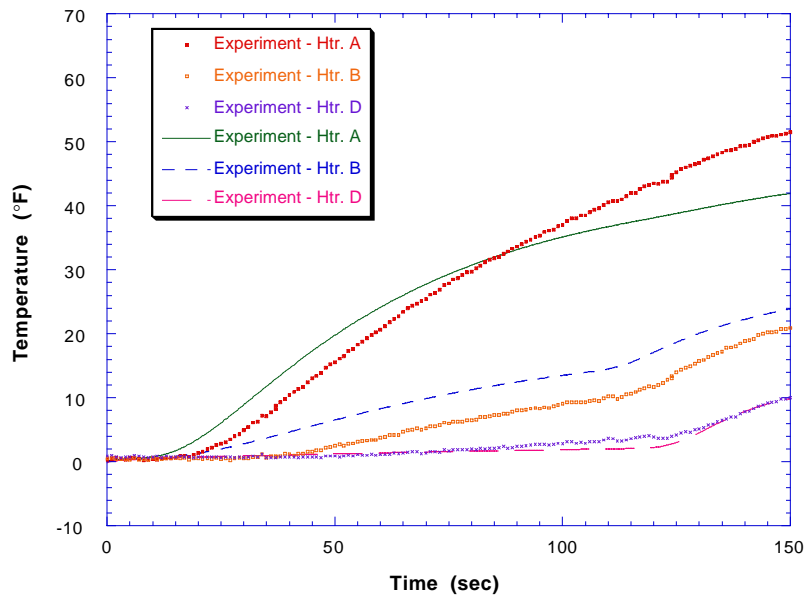
FIGURE 18. Foam Temperature Comparison for Case 3
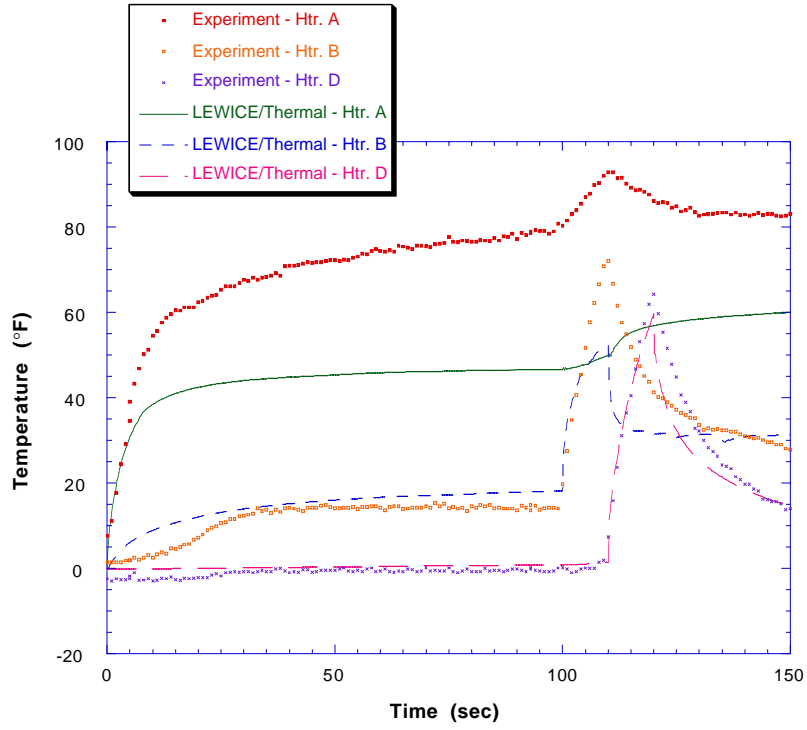
FIGURE 19. Heater Temperature Comparison for Case 4
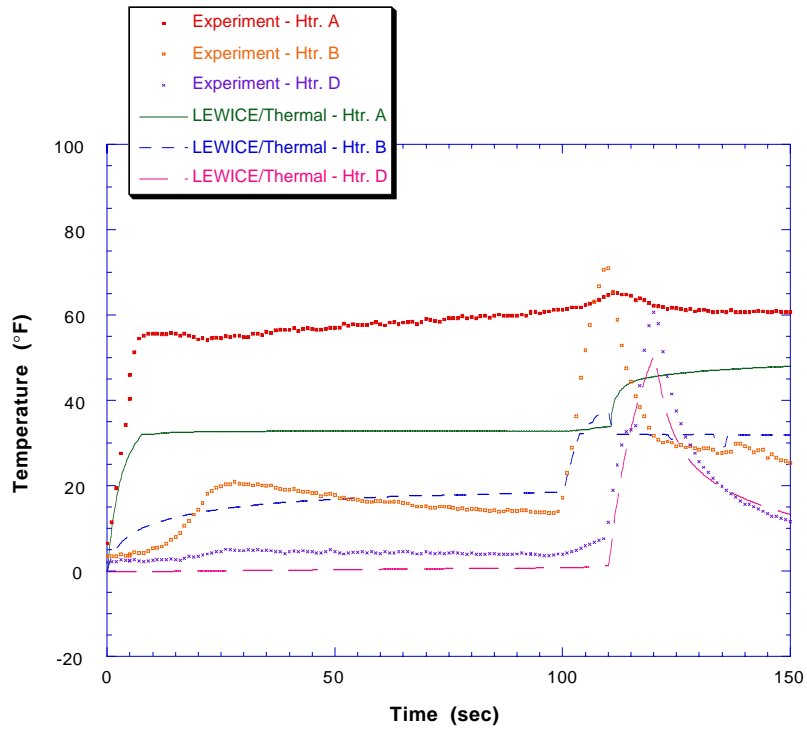
FIGURE 20. Surface Temperature Comparison for Case 4
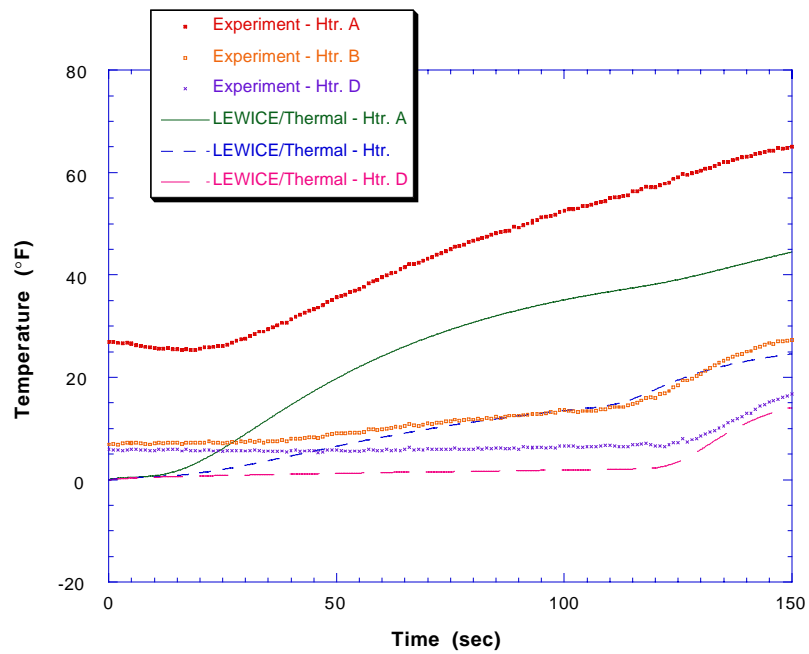
FIGURE 21. Foam Temperature Comparison for Case 4